

D. J. Dickrell III

University of Florida,
Mechanical Engineering Department,
Gainesville, FL 32611

D. B. Dooner

University of Puerto Rico,
Mechanical Engineering Department,
Mayaguez, PR 00681-9045

W. G. Sawyer

University of Florida,
Mechanical Engineering Department,
Gainesville, FL 32611

The Evolution of Geometry for a Wearing Circular Cam: Analytical and Computer Simulation With Comparison to Experiment

The evolution of the geometry of a simple two-dimensional circular cam as a result of wear is studied using three complementary approaches: a closed form analytical expression, a computer simulation, and the development of an experimental apparatus. Experiments were run for over 1.5 million cycles, and measurements of cam shape and follower motion were recorded and compared favorably to the predictions of both techniques. Errors associated with an accelerated computational approach are discussed.

[DOI: 10.1115/1.1504092]

Introduction

Life prediction for dynamic systems is an important concern for machine designers to consider for technical and economic reasons. A better understanding of the manner in which components wear out can significantly aid engineers in design work.

A key issue in predicting component life that demands careful consideration is the coupling of wear and load in surface contacts. A simple extrapolation of wear properties at the initial cycles of a mechanism can greatly over-predict or under-predict the amount of wear realized in that component's life due to the ever-evolving contact conditions at the interface. Several prediction methods are available that take this coupling into account.

Numerical studies, which include the finite-element method (FEM), have been used to simulate wear *in silico*. Podra and Andersson [1] published a thorough investigation of sliding-wear using FEM. The iterative nature of numerical simulations enables them to encompass the changing loads and geometries in the contact region, therefore modeling wear processes accurately. Another advantage of numerical simulation is the capability to rapidly change test conditions and component properties without inordinate set-up cost or significant downtime. One downside to these numerical processes is that through certain refinements of the numerical simulation, the model can become more costly and more time consuming than physical testing. Many studies are more thoroughly reviewed in papers by Blanchet [2] and Sawyer [3].

An alternate approach first proposed by Blanchet [2], and followed by Sawyer [3], is the development of a closed-form analytical expression for simple mechanisms using a simple line removal term for wear. These expressions are less common than other approaches due to their exclusivity to certain types of problems. For those special problems however, these closed-form expressions have proven extremely effective at predicting wear behavior [4].

Sawyer et al. [4] and Dinc et al. [5] developed test rigs to physically verify data generated by wear modeling. These rigs are important checks for model validity. The results produced by numerical or analytical models are relatively abstract without experimental data to reaffirm or contradict the predictions.

This paper describes the development of both analytical and numerical models to describe wear in a simple kinematic system,

an eccentrically mounted circular cam-follower mechanism. A summarization of the construction for an experimental rig to compare the model data is included as well. The error-differences between the numerical and analytical models are also discussed.

Experimental Setup

A cam-follower test rig was developed to experimentally quantify the coupled evolution of wear and load in the mechanism. The rig's overall construction can be seen in Fig. 1, while the contact geometry can be seen in Fig. 2.

The cam was CNC milled from a block of polytetrafluoroethylene (PTFE). The circular cam measured 38.1 mm in radius, 9.5 mm thick, and had a 6.35 mm eccentricity. The follower counterface wear surface was made of 17-7 PH stainless steel and had an initial average roughness of $R_a=2.1$ micrometers. The follower shafts were made of stainless steel and slid on solid-lubricated PTFE bushings. Two 17 N/mm compression springs located behind the follower face provided the necessary normal force. An initial target pre-load of 43 N was set at the point of minimum cam radius. Thus, the spring force varied from roughly 43 N to 259 N during the initial cycle. The corresponding maximum initial contact pressure was ~ 11.5 MPa.

The cam was mounted directly on the gear reduction shaft via a keyway. The electric motor was capable of rotational speeds of 1750 rpm, but a 10:1 gear reducer limited the rig's highest capable

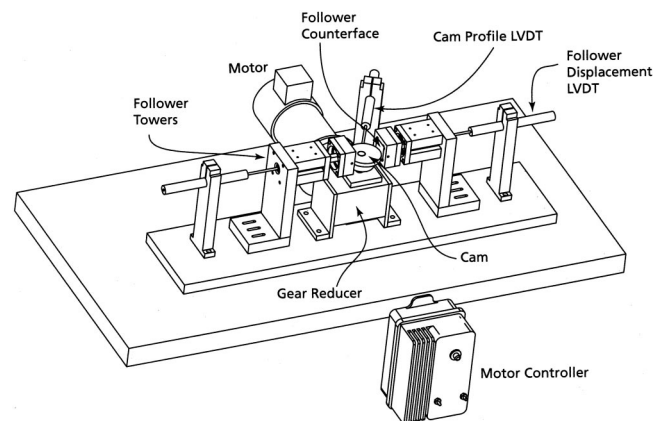


Fig. 1 Schematic of the cam follower experimental test rig. The two follower configuration gives 2 cycles per cam revolution.

Contributed by the Tribology Division of the THE AMERICAN SOCIETY OF MECHANICAL ENGINEERS for presentation at the ASME/STLE Tribology Conference, Cancun, Mexico October 27–30, 2002. Manuscript received by the Tribology Division February 7, 2002 revised manuscript received June 26, 2002. Associate Editor: M. D. Bryant.

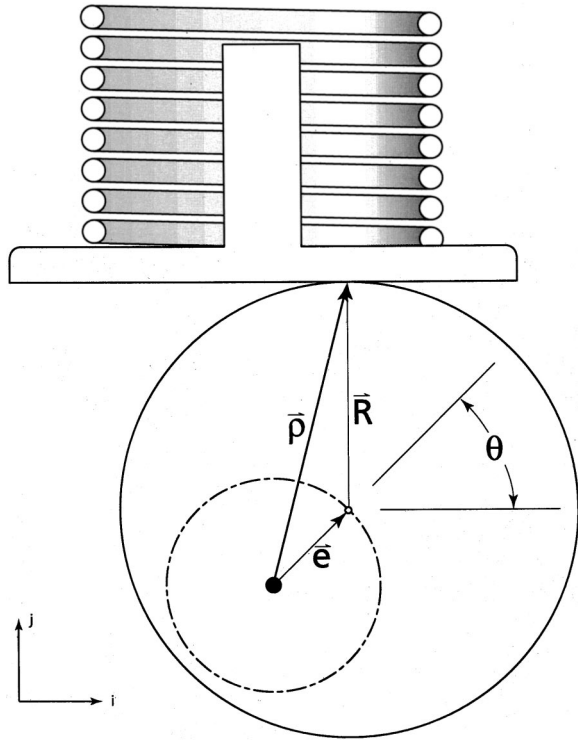


Fig. 2 Schematic and nomenclature for the simple eccentric-mounted circular cam

shaft speed to 175 rpm. The rotational speed was constrained to a certain range to minimize dynamic forces. The speed used during the experiment was maintained constant at 114 rpm. Due to the analytical model assumption of quasi-static conditions, efforts were made to minimize the follower mass. The follower mass of 629.5 grams corresponds to peak dynamic loads of approximately 1/2 N during the first cycle and reduces from there for subsequent cycles; this dynamic force is roughly 2 orders of magnitude less than the spring forces.

The materials selected for the cam and follower surface were chosen to maximize the material hardness difference so that follower wear could be neglected. The counter-face wear surface was also roughened to increase wear per cycle and reduce the total run-time. The remaining materials used to construct the support towers, base plate, and follower housing were aluminum.

During testing, a linear variable differential transformer (LVDT) measured each follower position and velocity while another directly measured the cam profile. This data was collected using a computerized data-acquisition system and saved periodically to a spreadsheet program. For a more detailed measurement, a freehand coordinate measuring machine (CMM) was used to measure the cam profile both before and after the experiment.

The experiment was run for 6830 minutes and the cam saw 1.56 million cycles of wear. The wear-rate (K) for PTFE on stainless steel was experimentally found to be $8.62 \times 10^{-4} \text{ mm}^3/(\text{Nm})$ using a reciprocating pin-on-disk apparatus under steady sliding speeds of 10 cm/s and an average contact pressure of 10 MPa on the same surface as the follower surface. This constant was used for all model predictions and no curve fitting was performed.

Analytical Modeling

A closed form analytical representation for the coupled evolution of geometry and contact loading as a result of wear for an eccentric circular-cam running on a flat-faced follower is derived. The cam-follower mechanism is treated as a two-dimensional disk running against a flat plate. The cam has a radius (R) from its

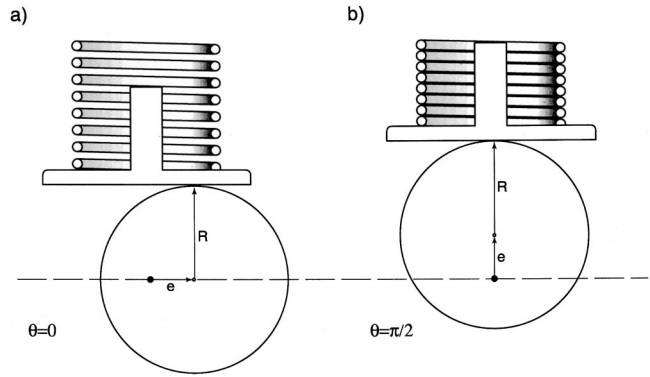


Fig. 3 Illustration of two configurations of interest for the analytical modeling (a) wear proceeds directly along the cam radius, and (b) wear proceeds along the cam radius and the eccentricity vector

geometric center, eccentricity (e) from the center of rotation to the geometric center, and a width of (w), these variables are constants taken from initial cam design and have units of length. The total wear of the system is solely partitioned to the cam (i.e., wear of the follower is ignored). An angular coordinate (θ) is used to express the contact conditions for all rotations in respect to a fixed coordinate system.

The closure equation for the eccentric circular cam with a flat-faced follower is shown in Eq. 1 and can be seen in Fig. 2.

$$\vec{\rho} = \vec{e} + \vec{R} = e \cos \theta \hat{i} + e \sin \theta \hat{j} + R \hat{j} \quad (1)$$

In this equation $\vec{\rho}$ is the vector from the center of rotation of the cam to the point of contact on the follower, \vec{e} is the vector from the center of rotation to the geometric center of the cam, and \vec{R} is the radial vector from the geometric center of the cam to the point of contact on the follower. The unit vectors \hat{i} and \hat{j} are shown in Fig. 2. Assuming that a circular cam remains circular, two specific locations on the cam can be used to describe the wear for the entire cam surface. These special positions, $\theta=0$ and $\theta=\pi/2$, are illustrated in Fig. 3. Following the models of previous studies [1–4], the wear-depth at each location on the cam is treated as proceeding perpendicularly inward from the line of contact.

The spring deflection for $\theta=0$ is denoted as d_0 , and the spring force is $F_n = kd_0$. Using the expression for the line wear-depth $\Delta_1 = KF_n/w$ [2–4], the first and second cycle wear depth at the $\theta=0$ location is given by Eqs. 2 and 3.

$$\Delta_1 = \frac{Kkd_0}{w} \quad (2)$$

$$\Delta_2 = \frac{Kk}{w} \left(d_0 - \frac{Kkd_0}{w} \right) \quad (3)$$

The wear of the following cycle is affected by the previous cycle's reduction of the spring force due to the diminution of the spring deflection. The wear depth at the $\theta=0$ location proceeds as a summation of cycles. For any cycle N , the wear is given by Eq. 4.

$$\Delta_N = \frac{Kk}{w} d_0 \left(1 - \frac{Kk}{w} \right)^{N-1} \quad (4)$$

The Kk/w term is dimensionless and is given the designation β^* . The Δ_N expression for each cycle must be summed to account for the total amount of wear realized at the $\theta=0$ location. The total wear at $\theta=0$ for cycle number n is given in Eq. 5.

$$\Delta_{\text{total}} = \sum_{N=1}^n \Delta_N = \sum_{N=1}^n \beta^* d_0 (1 - \beta^*)^{N-1} = d_0 [1 - (1 - \beta^*)^n] \quad (5)$$

The \vec{R} vector at $\theta=0$ for any number of cycles can be expressed as a function of the initial radius R_0 and the total wear for that cycle. Thus the magnitude of the radial vector (R) from the center of the cam to the point of contact for any arbitrary number of cycles can be expressed as Eq. 6.

$$R = R_0 - \sum_{N=1}^n \Delta_N = R_0 - d_0[1 - (1 - \beta^*)^n] \quad (6)$$

This can be nondimensionalized by dividing through by the initial radius R_0 , and introducing the R^* and d^* which are the quotients of R/R_0 and d_0/R_0 , respectively. The nondimensional form of the decay equation of the magnitude of the radial vector as a function of cycle number n is given by Eq. 7.

$$R^* = 1 - d^*(1 - (1 - \beta^*)^n) \quad (7)$$

The analysis now proceeds to the $\theta = \pi/2$ location where the \vec{e} vectors' contribution to the spring deflection (D) is maximal $D = d_o + e$. Since the spring deflection directly maps to the amount of wear the cam has undergone, the spring deflection decays in the same manner described in Eq. 6. Thus, the eccentricity (e) decays in a similar manner. The spring deflection at the $\theta = \pi/2$ location as a function of the initial spring deflection at this location is given by Eq. 8.

$$D_n = D_o - D_o[1 - (1 - \beta^*)^n] \quad (8)$$

Equation 8 can be partitioned into its d and e components, $D_n = d_n + e_n$ and $D_o = d_o + e_o$. Making these substitutions, Eq. 8 can be rearranged into Eq. 9.

$$d_n + e_n = d_o - d_o[1 - (1 - \beta^*)^n] + e_o - e_o[1 - (1 - \beta^*)^n] \quad (9)$$

Since $d_n = d_o - d_o[1 - (1 - \beta^*)^n]$, Eq. 8, can be further reduced. Normalizing the equation by the initial eccentricity e_o and introducing the e^* , which is the quotient of e_n/e_o , gives Eq. 10, the nondimensional decay equation for the eccentricity.

$$e^* = 1 - [1 - (1 - \beta^*)^n] = (1 - \beta^*)^n \quad (10)$$

Using Eqs. 7 and 10, the shape and motion for the circular cam can be expressed as a function of the number of cycles.

Computer Simulation

The examination of more generalized and complicated cam-profiles necessitates the use of a numerical scheme to examine the coupling of wear and load. The "classical" synthesis of a cam surface involves the determination of the cam coordinates necessary to produce a predetermined follower motion, $s(\theta)$, (i.e., the follower motion generates a profile from which the cam is constructed). In order to do this, some kinematic arguments need to be made. Figure 4 depicts a cam in contact with a flat-faced follower, a fixed coordinate system (X, Y), a cam attached coordinate system (x, y), the angular position θ between (X, Y) and (x, y), the base circle radius R_b , and the point of contact c .

The *theorem of instant centers* or the *Arnold-Kennedy instant center theorem* is used in this approach. The theorem states that given any two instant centers (planar motion), the third instant center must lie on a line connecting the two known instant centers. As for the case of a two-dimensional cam and flat-faced follower, the instant center between the cam and ground $IC_{c,g}$ is located at the center of rotation of the cam (the origin of the fixed coordinate system (X, Y)). The instant center of the follower and ground $IC_{f,g}$ lies infinitely far away from the follower face perpendicular to the direction of travel. Thus, the instant center $IC_{c,f}$ between the cam and follower must lie on the line connecting the two instant centers, which can only be a location somewhere along the X -axis.

The velocity of the follower is given by Eq. 11 below, and by virtue of the instant center theorem, the X coordinate of the contact point (X_c) is given by Eq. 12, the Y coordinate of the contact point (Y_c) requires no clever derivation and is given by Eq. 13.

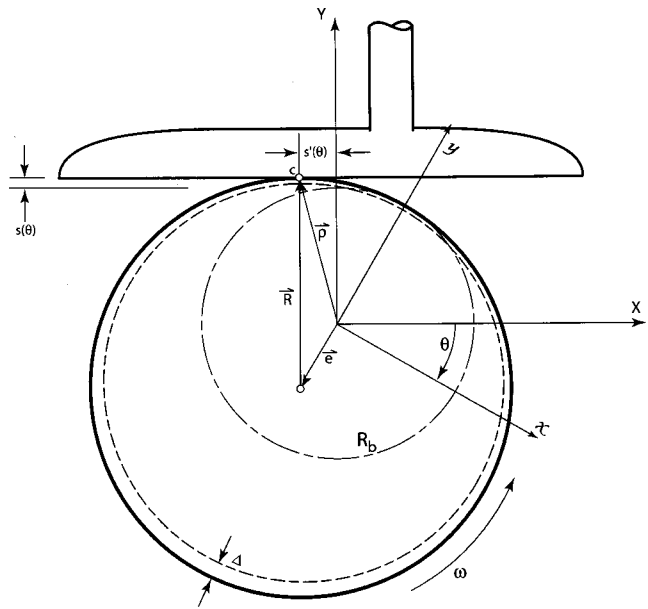


Fig. 4 Schematic and nomenclature for the computer simulation

The nomenclature is, $\dot{s}(\theta)$ is the derivative of the dependent variable s with respect to time and $s'(\theta)$ is the geometric derivative of s with respect to θ .

$$\dot{s}(\theta) = \omega s'(\theta) \quad (11)$$

$$X_c \omega = \dot{s}(\theta) = \omega s'(\theta), \therefore X_c = s'(\theta) \quad (12)$$

$$Y_c = R_b + s(\theta) \quad (13)$$

These coordinates, parameterized in the fixed coordinate system, must be re-parameterized in the moving coordinate system to establish a meaningful representation of the cam surface. The cam surface is parameterized in a clockwise manner for a positive CCW rotation of the cam itself using an array of the contact coordinates. Consequently, these coordinates in the moving coordinate system (x, y) can be represented in matrix form as

$$\begin{Bmatrix} x_c \\ y_c \end{Bmatrix} = \begin{bmatrix} \cos \theta & \sin \theta \\ -\sin \theta & \cos \theta \end{bmatrix} \begin{Bmatrix} X_c \\ Y_c \end{Bmatrix} \quad (14)$$

As the cam and follower mesh together, both surfaces wear. The depth of wear at the contact can be predicted as discussed previously using Archard's wear equation. Typically, followers are held in contact with the cam using a spring. For a constant speed cam the contact force (F_n) is given by Eq. 15, where F_0 is the preload, (k) is the spring constant, $s(\theta)$ is the follower motion, m is the mass of the follower, and ω is the angular speed of the cam.

$$F_n = F_0 + ks(\theta) + m\omega^2 s''(\theta) \quad (15)$$

For the case where the follower wear is negligible, only the cam surface experiences a change in geometry. Assuming that the wear proceeds perpendicular to the cam surface the new cam surface coordinates (\bar{x}_c, \bar{y}_c) after one wear cycle can be expressed by Eqs. 16 and 17, where the surface tangent vector has \hat{i} and \hat{j} components of x'_c and y'_c .

$$\bar{x}_c = x_c + \Delta \frac{y'_c}{\sqrt{(x'_c)^2 + (y'_c)^2}} \quad (16)$$

$$\bar{y}_c = y_c - \Delta \frac{x'_c}{\sqrt{(x'_c)^2 + (y'_c)^2}} \quad (17)$$

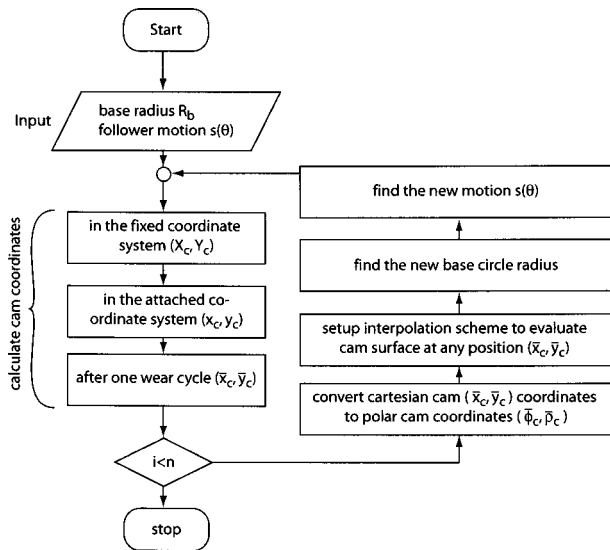


Fig. 5 A flowchart for the computer simulation

For the case of an eccentrically mounted circular cam, the motion $s(\theta)$ and its derivative $s'(\theta)$ can be expressed as $s(\theta) = e(1 - \cos \theta)$, and $s'(\theta) = e \sin \theta$, where e is the eccentricity. Substituting these expressions for motion into Eqs. 16 and 17 gives the following expression for the worn cam surface coordinates.

$$\bar{x}_c = [(R_b + e) - \Delta] \sin \theta \quad (18)$$

$$\bar{y}_c = [(R_b + e) - \Delta] \cos \theta - e \quad (19)$$

Using Eq. 15, and neglecting the follower mass, the new cam points can be expanded and simplified into the form of the equation for a circle whose center is located a distance h along the y -axis $\bar{x}_c^2 + (\bar{y}_c + h)^2 = \bar{R}_b^2$. The cam shape remains circular if the wear $\Delta = 0$, and is centered about the point $(0, -e)$. The cam shape also remains circular if $e = 0$, and is centered about the point $(0, 0)$ with a radius that is given by

$$R = R_b - \frac{KF_o}{w} \quad (20)$$

Unfortunately, only for a select few cases does a circular cam remain circular and a general approach is required for even the simple case of an initially circular cam with a flat-faced follower.

Having obtained the new cam surface (\bar{x}_c, \bar{y}_c) for one wear cycle, it is necessary to determine its new base radius \bar{R}_b , which is the largest inscribed circle on the cam geometry about the center of rotation, and the matching motion $\bar{s}(\theta)$ that corresponds to the new cam surface. The coordinates (\bar{x}_c, \bar{y}_c) are no longer available for use as an explicit expression but rather as discrete data. Consequently, a cubic-spline interpolation scheme to determine the cam coordinates for the regions between the desired discrete data points is employed. The Cartesian coordinates of the cam surface (\bar{x}_c, \bar{y}_c) are converted to polar coordinates $\bar{\phi}_c$ and $\bar{\rho}_c$ using Eqs. 21 and 22.

$$\bar{\phi}_c = \tan^{-1} \left(\frac{\bar{y}_c}{\bar{x}_c} \right) \quad (21)$$

$$\bar{\rho}_c = \sqrt{\bar{x}_c^2 + \bar{y}_c^2} \quad (22)$$

The interpolation scheme determines the new base radius \bar{R}_b by minimizing the relation shown in Eq. 23 via the Golden Section search method.

$$f_1(\bar{\rho}_c) = \sqrt{\bar{x}_c^2 + \bar{y}_c^2} \quad (23)$$

It is necessary to determine the coordinates (\bar{x}_c, \bar{y}_c) for a specified CCW angular displacement θ of the cam. The radial unit vector \hat{a}

at an angle θ is $\hat{a} = (\sin \theta, \cos \theta, 0)$, and the unit tangent vector \hat{b} along the cam surface is $\hat{b} = (\bar{x}'_c, \bar{y}'_c, 0)$. Thus, the cam coordinates (\bar{x}_c, \bar{y}_c) that correspond to the position θ are determined by the condition $\hat{b} \cdot \hat{a} = 0$, and consequently the new follower motion can be determined. A flowchart for this computer simulation is shown in Fig. 5. The simulation marches forward to a target number of cycles and periodically writes both the cam shape and follower motion to a text file.

Extrapolation

The numerical simulation code is not optimized in any way for speed, and running with 1000 surface points on a 500 MHz single processor workstation it takes approximately 20s to simulate a single wear cycle. This is over an order of magnitude slower than the time required to physically run a cycle on the experimental apparatus. Thus, it is obviously desirable to simulate 1.5 million cycles with considerably less computational cycles.

Based on Eq. 10, the errors associated with trading wear-rate for number-of-cycles is investigated. A multiplication factor (a) was applied to accelerate the rate-of-wear. The errors associated with increasing the wear rate 10,000 fold and thereby decreasing the number of compute cycles a corresponding 10,000 fold is examined using Eq. 24. The denominator is the extrapolated solution. The error as a function of number of cycles is shown in Fig. 6, using the values for k , K , and w given previously in the Experimental section.

$$\text{error Fraction} = \frac{\left(1 - \frac{kK}{w}\right)^n}{\left(1 - \frac{k(aK)}{w}\right)^{n/a}} = \frac{(1 - \beta^*)^n}{(1 - a\beta^*)^{n/a}} \quad (24)$$

As shown in Fig. 6, the error associated with this type of extrapolation is only slightly more than 1 percent after 1.5 million cycles. Thus, the entire range could be simulated by performing only 150 compute cycles, about 50 minutes of computation.

Results and Discussion

Figure 7 compares the experimental, analytical, and numerical results for R and e versus cycle number. Although simple analysis

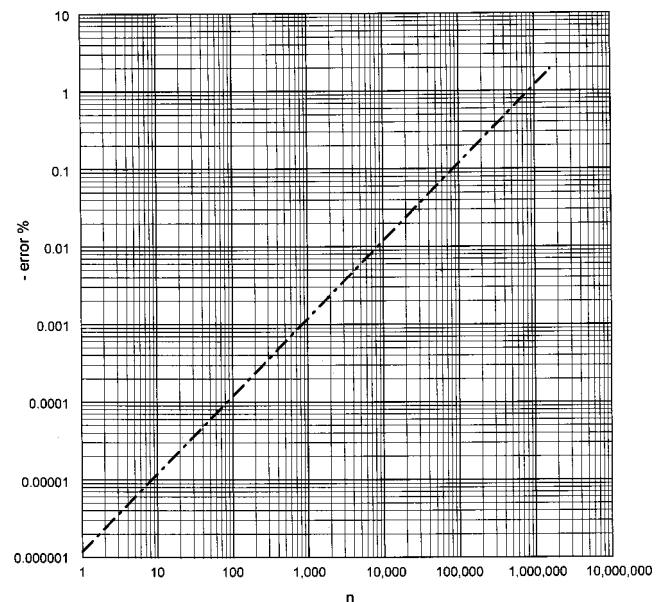


Fig. 6 Error estimation using a wear-rate 10,000x greater than the experimentally determined value as a function of number of cycles

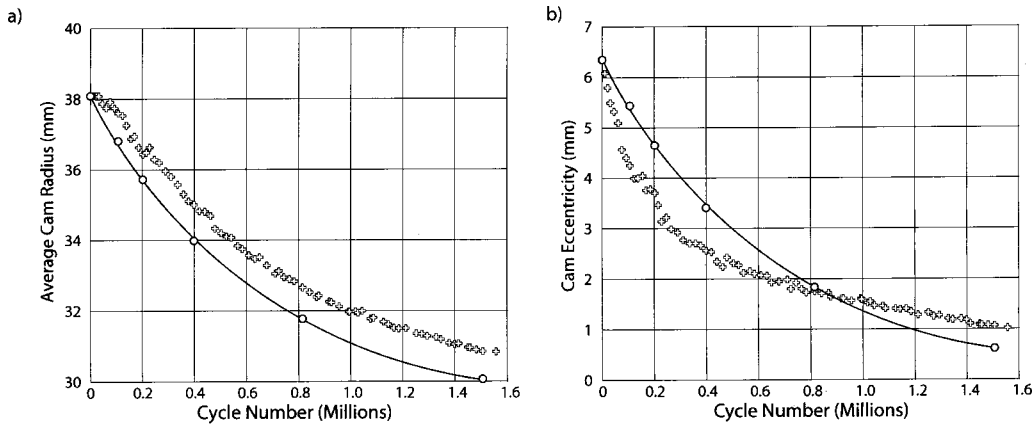


Fig. 7 Comparison between the measured (crosses), analytical predictions (curve), and the computer simulation (○) for (a) the average radius of curvature, and (b) the cam eccentricity

shows that the cam is not exactly a circle the results from the numerical solution are virtually indistinguishable from a circle. Figure 8 plots the worn cam profile coordinates from the CMM after 1.56 million cycles. Overall, the numerical model with the accelerated wear-rate, the analytical model with the assumed circular wear shape progression, and the experiment are in close agreement. The difference between the predicted shape and the measured shape is within 3 percent.

Better agreement between the models and the experimental results could be obtained by fitting a wear-rate to the experimental results. However, the intention of this study was to investigate the suitability of making predictions of a wearing mechanism's performance without having to perform such curve fitting, using parameters gathered from other more simple laboratory measurements. Thus, no parameters were fit to the data, and the good

agreement is encouraging. There are some differences between the shapes of the measured and predicted R and e curves; perhaps this suggests the need for cycle dependent wear rates in future modeling.

The inclusion of wear in computer simulations is very computationally expensive. While computer speed will continue to increase in the coming years it is very unlikely that each cycle of an expected product life can be simulated for the vast majority of mechanisms and components of interest to engineers. Thus, the usage of some sort of accelerated wear rate is recommended, and it is hoped that simple closed form analytical approaches such as these offered here can guide such extrapolations. The risk of accelerated wear is gross errors in the predictions, as an example, Fig. 9 shows the predicted shape at 1.5 million cycles after accelerating wear 1,500,000x, i.e., extrapolating wear from the first cycle. There is no agreement between this shape and the actual shape of the cam after this many cycles.

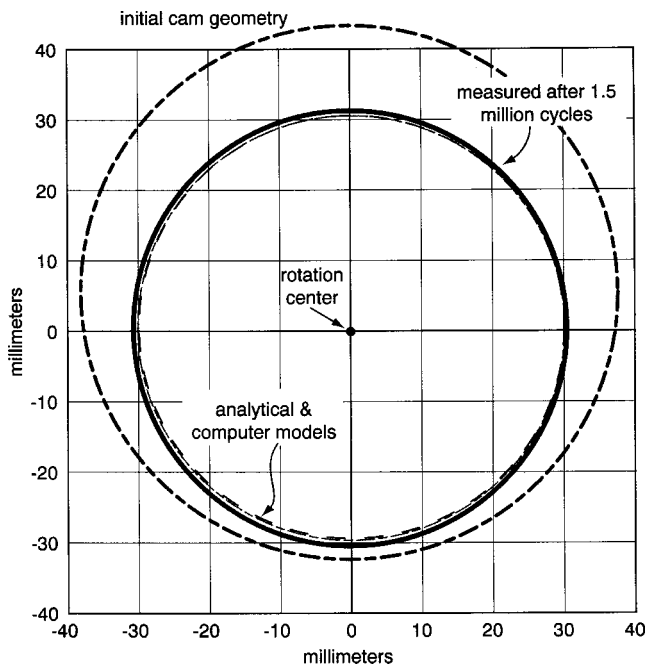


Fig. 8 Comparisons between the measured, analytical, and computer simulation for the cam shape

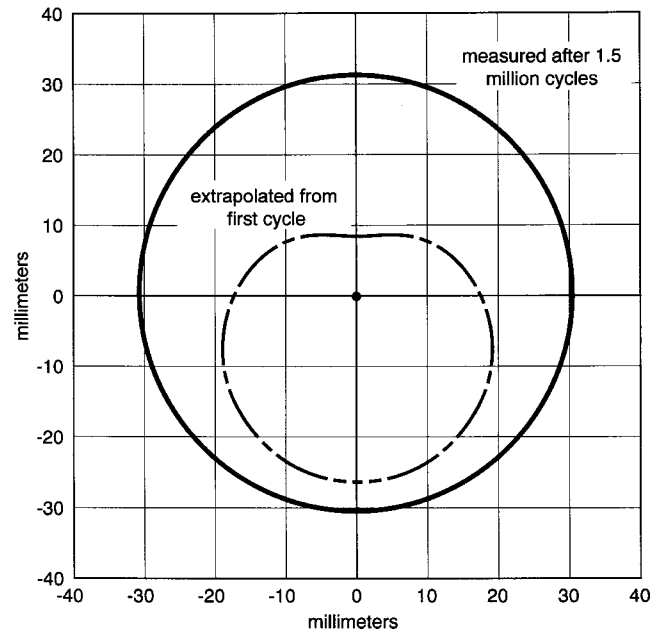


Fig. 9 Comparison between the extrapolated shape from cycle 1 and the measured shape

Closure

1 The predictions of the closed form analytical solution and the accelerated computer simulation were in agreement better than 1 percent.

2 The predictions of cam shape and motion were in agreement with the experiment without any fitting of parameters to better than 3 percent. Under certain conditions, accelerated wear-rates can be used in numerical simulations without excessive errors in the predictions.

References

- [1] Podra, P., and Andersson, S., 1999, "Simulating Sliding Wear With Finite Element Method," *Tribol. Int.*, **32**, pp. 71–81.
- [2] Blanchet, T. A., 1997, "The Interaction of Wear and Dynamics of a Simple Mechanism," *ASME J. Tribol.*, **119**, pp. 597–599.
- [3] Sawyer, W. G., 2001, "Wear Predictions for a Simple-Cam Including the Coupled Evolution of Wear and Load," *Lubr. Eng.*, pp. 31–36.
- [4] Sawyer, W. G., Diaz, K. L., Hamilton, M. A., and Micklos, B., 2001, "Evaluation of an Analytical Model for the Evolution of Wear and Load in a Scotch-Yoke Mechanism," *ASME J. Tribol.*, submitted to the *Journal of Tribology*.
- [5] Dinc, O. S., Cromer, R., and Calabrese, S. J., 1995, "Redesigning Mechanical Systems for Low Wear Using System Dynamics Modeling," *ASME J. Tribol.*, **35**, pp. 1–8.